Micromechanics of Thermoelastic Behavior of AA6070 Alloy/Zirconium Oxide Nanoparticle Metal Matrix Composites

Chennakesava R Alavala

Department of Mechanical Engineering, JNT University, Hyderabad-500085, India

Abstract— *The present work was deliberated to predict thermoelastic behavior of AA6070 alloy / ZrO_2 nanoparticle metal matrix composites. ZrO_2 is used is used in composite cutting tools and abrasive wheels. The RVE models were used to analyze thermo-elastic behavior. The stiffness of AA6070 alloy / ZrO_2 nanoparticle metal matrix composites decreased with the increase of temperature. ZrO_2 nanoparticles had undergone thermal shock at 300^oC. The fracture was noticed at the interphase between AA6070 alloy and ZrO_2 nanoparticles.*

Keywords— AA6070 alloy, zirconium oxide, RVE model, thermoelastic, finite element analysis.

I. INTRODUCTION

Metal matrix composites consisting aluminum alloy matrix and nanoparticulate reinforcements, also termed 'nanocomposites', have fascinated the attention of researchers because of the enormous guarantee they give as novel structural materials. Nanocomposites, in broad, have been the subject of thorough investigation in recent years, and considerable progress has been made in the processing and in understanding of their essential properties. By reinforcing an aluminum alloy with nanoparticulates of stronger and stiffer material such as SiC [1-4], alumina [5, 6], alumina trihydrate [7], aluminum nitride [8] or carbon [9, 10], it is feasible to manufacture a composite that conserves the light weight of the aluminum alloy while achieving greater strength and stiffness.

Thermal decomposition kinetics and interaction of thermal energy between particulate and matrix are of the essence for durability of nanocomposites for high temperature applications. Zirconium oxide (ZrO_2) has elastic modulus of approximately 250 GPa and CTE (coefficient of thermal expansion) of 12.2 μm/m-^oC. Because of high strength and fracture toughness coupled with high hardness, zirconia is used in composite cutting tools and abrasive wheels. AA6070 alloy has elastic modulus of 69 GPa, shear modulus of 26 GPa and CTE of 23.2 μm/m-^oC. AA 2024 alloy is used for motorbike or bicycle frames and armored vehicles. AA6070 alloy is used in manufacturing pipelines and heavy duty welded structures. For composites consisting of nanoparticles, the strengthening could be mainly attributed to the Orowan and the Hall–Petch strengthening mechanisms [11]. The significance of the direct and indirect strengthening is dependent on both the interparticle spacing of the reinforcement and the grain size of the matrix material. In recent years, it has been proven the use of finite element method (FEM) coupled with a unit cell model of the nanocomposites for this purpose [12].

The present work was to explore the thermoelastic behavior of nanoparticulate ZrO_2/AA6070 alloy matrix composites. Finite element analysis (FEA) was executed to determine the local response of the material using representative volume element (RVE) reinforced by a single particle contingent on hydrostatic and isothermal loading.

II. MATERIAL AND METHODS

The matrix material was AA6070 alloy. The reinforcement nanoparticulate was ZrO_2 of average size 100nm. The mechanical properties of materials used in the current work are given in table 1. The volume fractions of ZrO_2 nanoparticles were 10% and 20%.

In this research, a square RVE (Fig. 1) was prepared to infer the thermo-elastic performance AA6070/ZrO_2 nanocomposites. The PLANE183 element was exploited in the matrix and the interphase regions in the RVE models. The interphase between nanoparticle and matrix was discretized with CONTACT172 element [13]. Both uniform thermal and hydrostatic pressure loads were activated concurrently on the RVE model.

TABLE 1
MECHANICAL PROPERTIES OF AA6070 MATRIX AND ZrO_2 NANOPARTICLES.

Property	AA6070	ZrO_2
Density, g/cc	2.71	3.54
Elastic modulus, GPa	69.0	330
Ultimate tensile strength, MPa	145	711
Poisson's ratio	0.33	0.32
CTE, µm/m-oC	23.2	12.2
Thermal Conductivity, W/m-K	171.0	2.7
Specific heat, J/kg-K	891	540

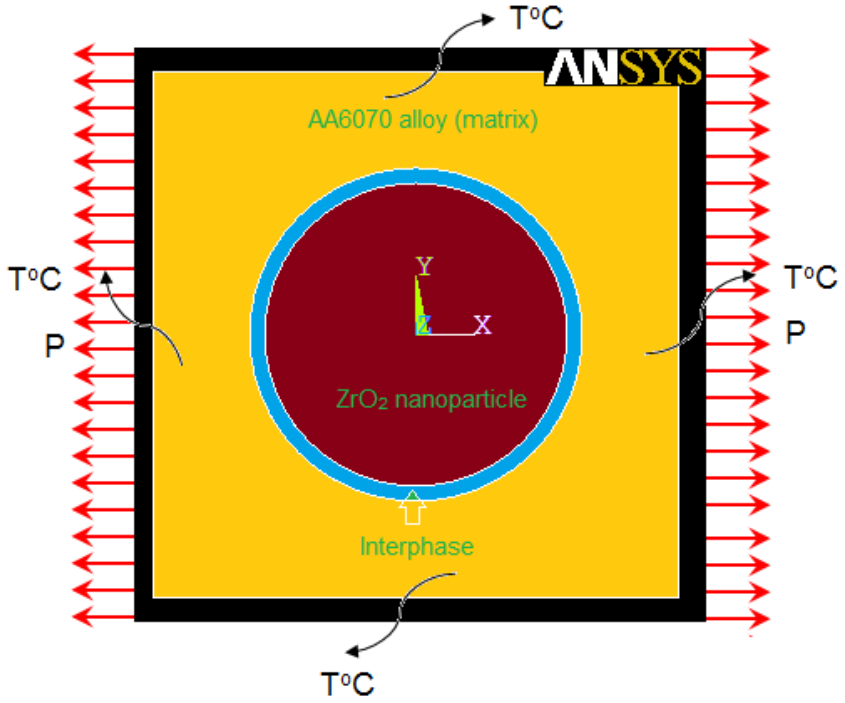

FIG.1. THE RVE MODEL

Poisson's ratio can have positive or negative values of large magnitude in anisotropic materials. For orthotropic materials, Poisson's ratio is bounded by the ratio of Young's moduli E as follows [14]:

$$|v12| < (Ex / Ey)1/2 \quad (1)$$

The other definition of major Poisson's ratio is as follows:

$$|v12| = - \varepsilon y / \varepsilon x \quad (2)$$

In the present work, Poisson's ratio v12 was computed to confirm the results.

III. RESULTS AND DISCUSSION

The finite element analysis (FEA) was conceded at 0°C to 300°C isothermal conditions. The hydrostatic pressure load was applied on RVE model to explore micromechanics of thermo-elastic tensile behavior of AA6070/ZrO_2 nanoparticulate composites. The volume fractions of ZrO_2 nanoparticles in the AA6070 matrix were 10% and 20%.

3.1 Micromechanics of thermo-elastic behavior

The dependence of thermo-elastic strains on temperature is showed in Fig. 2. The increase of temperature increased the strains. This trend was same for the strains along x- and y-directions. The strains were higher in the composites having 10%ZrO_2 than those having 20%ZrO_2. The maximum tensile strains had occurred in the direction of tensile loading as

showed in Fig. 3(a) and Fig. 4(a). The maximum compressive strains had cropped up in the transverse direction of tensile loading as showed in Fig. 3(b) and Fig. 4(b).

The stresses induced along x- and y-directions as a function of temperature are depicted in Fig. 5. They increased with the increase of temperature. Figs. 6 and 7 show raster images of stresses induced in the composites having 10% and 20% ZrO_2 nanoparticles, respectively. In the composites the maximum stress were occurred along the direction according to its type. The maximum was induced either in the nanoparticle or in the interphase as observed from Fig. 6 and Fig. 7. The transfer of stresses increased with the increase of temperature from the matrix to the nanoparticle as seen from the order of colors. It is also observed that the interphase between the nanoparticle and matrix had experienced different local stress fields as indicated by the spectrum of different colors bands across it.

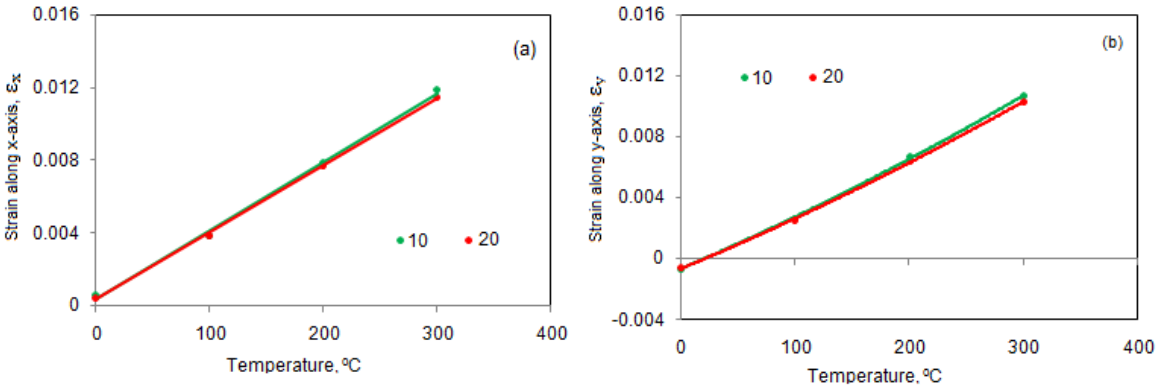

FIG. 2. INFLUENCE OF TEMPERATURE ON THERMOELASTIC STRAINS: (A) ε_x AND (B) ε_y.

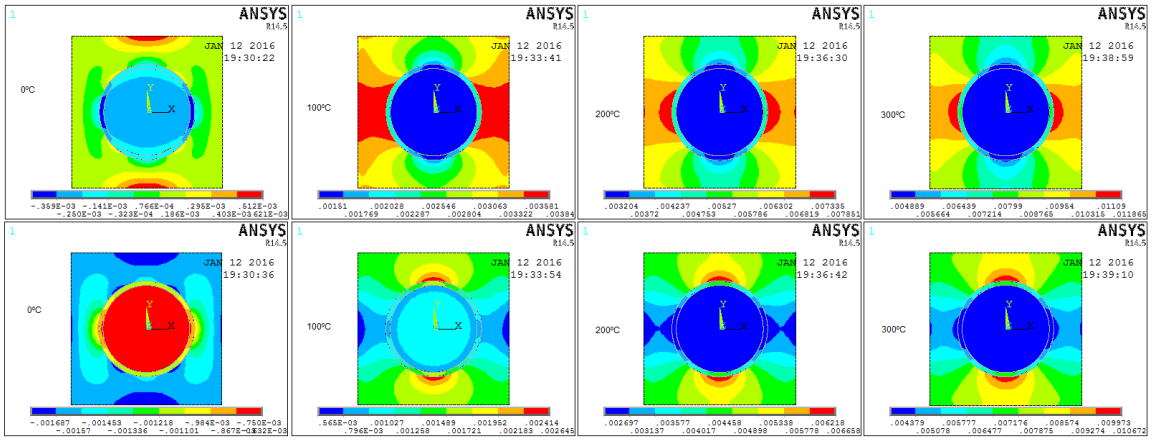

FIG. 3. RASTER IMAGES OF STRAINS OF AA6070/10%ZrO_2 COMPOSITES: (A) ε_x AND (B) ε_y.

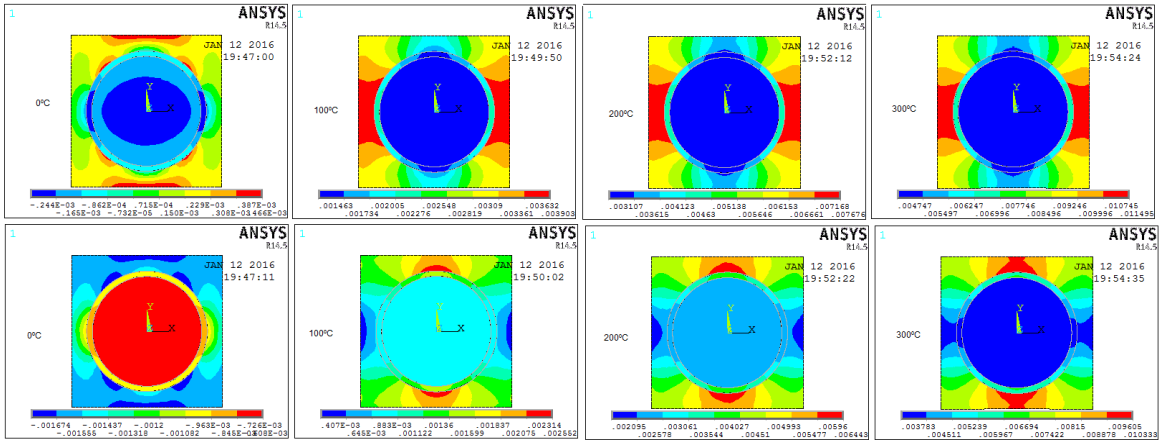

FIG. 4. RASTER IMAGES OF STRAINS OF AA6070/20%ZrO_2 COMPOSITES: (A) ε_x AND (B) ε_y.

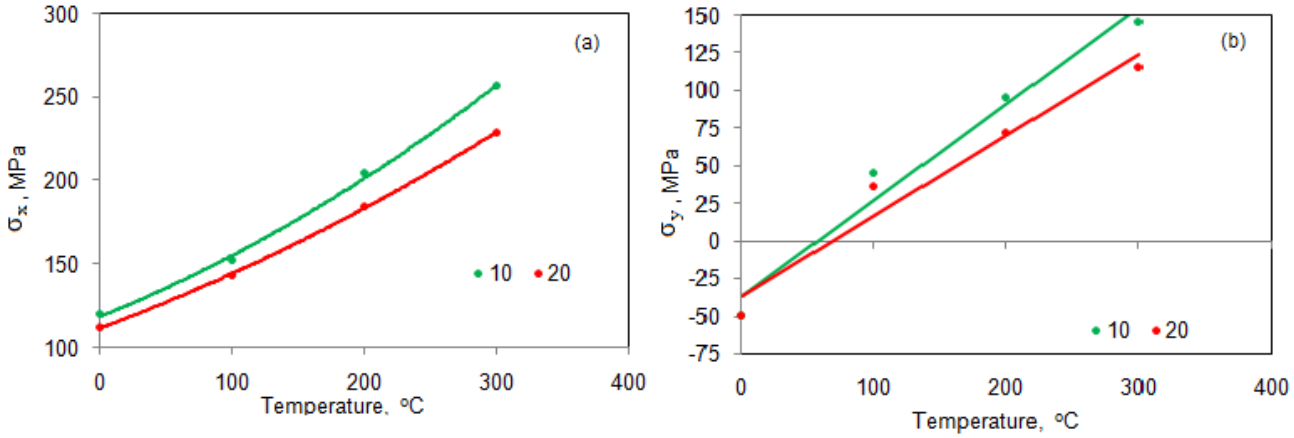

FIG. 5. INFLUENCE OF TEMPERATURE ON STRESS: (A) σ_x AND (B) σ_y

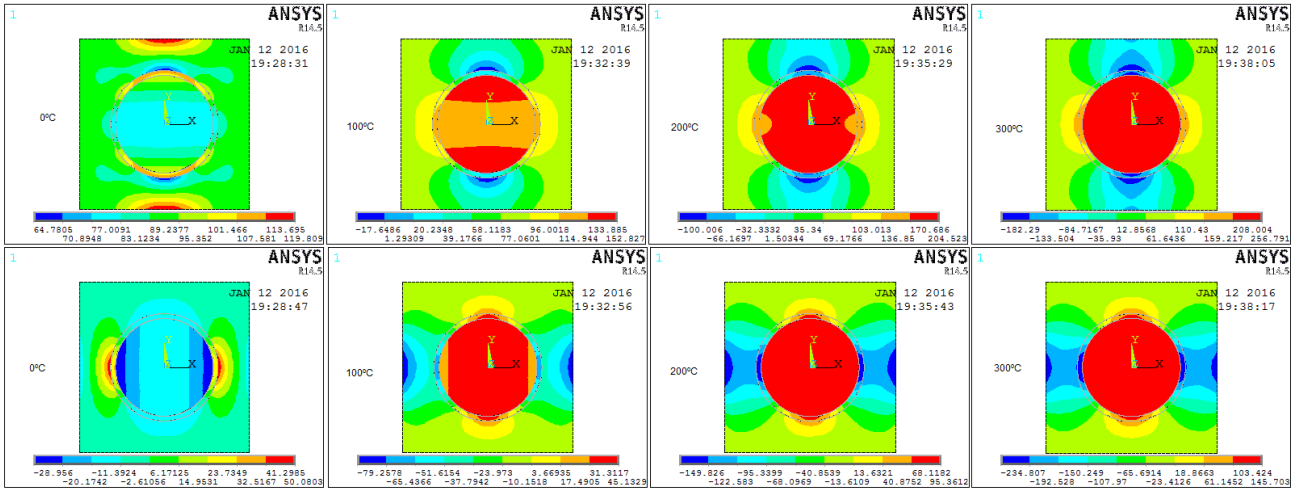

FIG. 6. RASTER IMAGES OF STRESSES INDUCED IN AA6070/10% ZrO_2 COMPOSITES: (A) σ_x AND (B) σ_y.

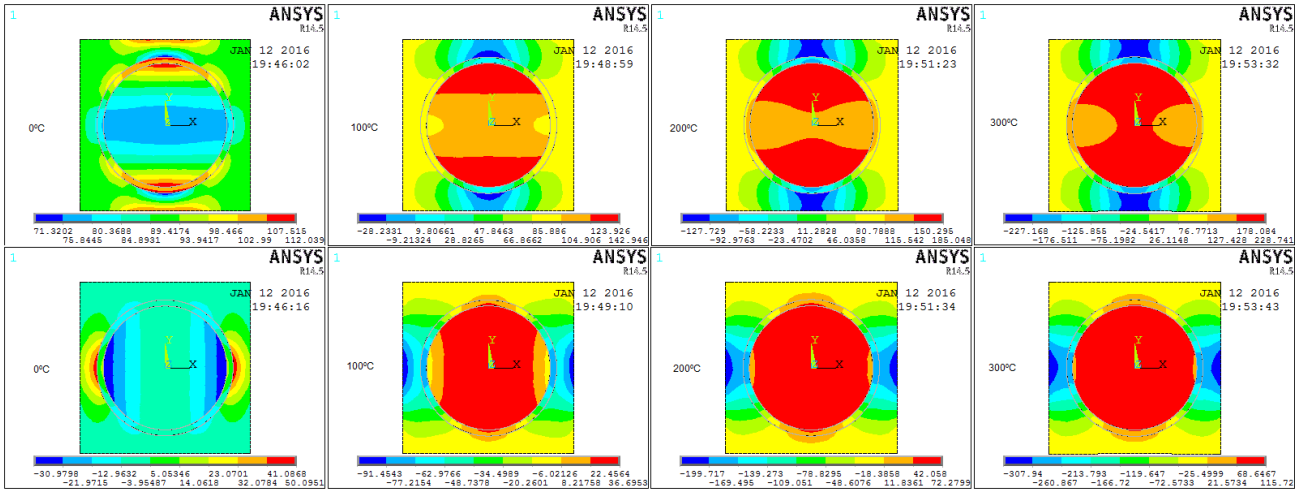

FIG. 7. RASTER IMAGES OF STRESSES INDUCED IN AA6070/20% ZrO_2 COMPOSITES: (A) σ_x AND (B) σ_y.

The elastic moduli decreased with the increase of temperature as showed in Fig. 8. The elastic modulus was higher along x-direction than that along y-direction. The elastic moduli in the composites having 20% ZrO_2 was higher than those of composites having 10% ZrO_2. This might be attributed to the stiffness of ZrO_2 nanoparticles. The ZrO_2 nanoparticles are very stiffer to undergo deformation under tensile loading. This phenomenon is also confirmed with the variation of major Poisson's ration with the temperature (Fig. 9). Poisson's ratio is bounded by the ratio of Young's moduli E as mentioned in Eq. (1).

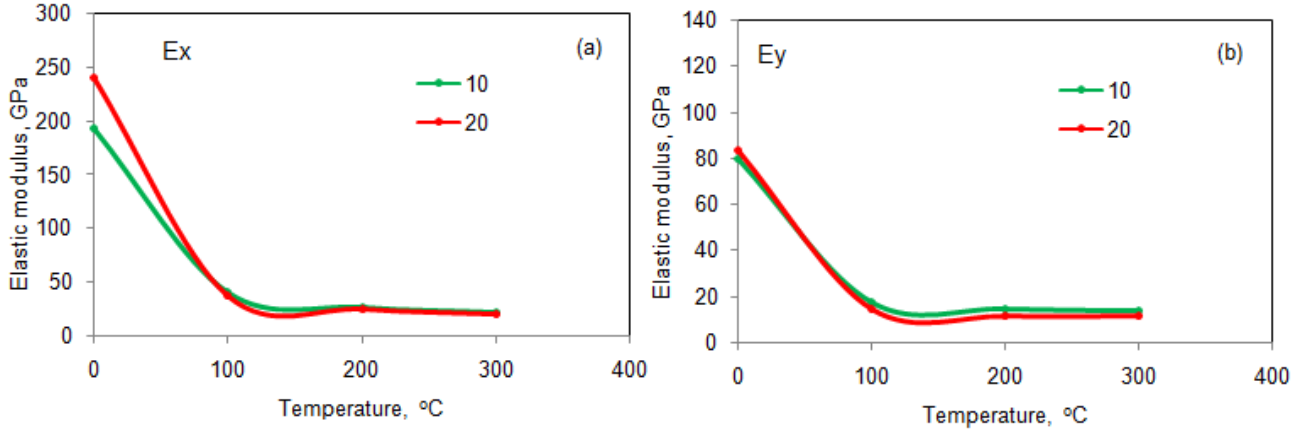

FIG. 8. INFLUENCE OF TEMPERATURE ON ELASTIC MODULUS: (A) E_x AND (B) E_y.

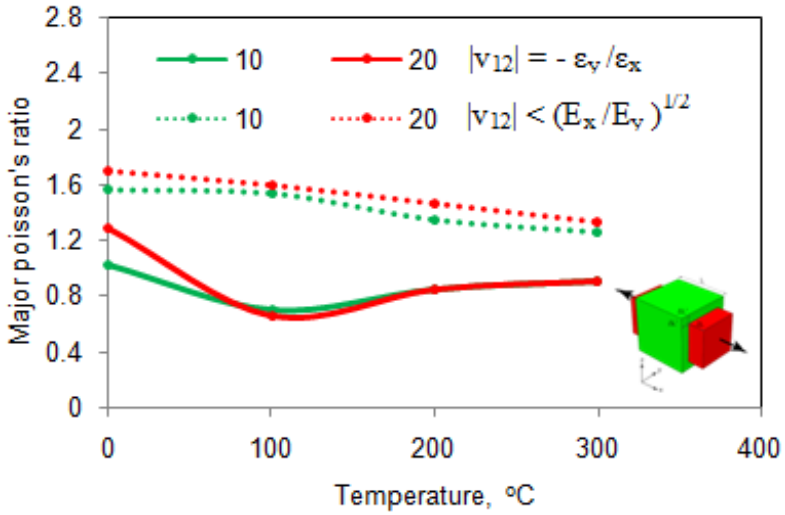

FIG. 9. INFLUENCE OF TEMPERATURE ON MAJOR POISSON'S RATIO

3.2 Fracture behavior

The shear and von Mises strains increased with increase of temperature as showed in Fig. 10. Neither ZrO_2 nanoparticle nor interphase experienced the failure von Mises strain but the matrix AA6070 alloy as illustrated in Fig. 11(a) and Fig. 12(a). The orientation of shear strain for the composites subjected to no isothermal (0^oC) loading was 135^o at the same time as it was 45^o for the temperatures from 100^oC to 300^oC as sighted in figure 11(b) and Fig. 12(b).

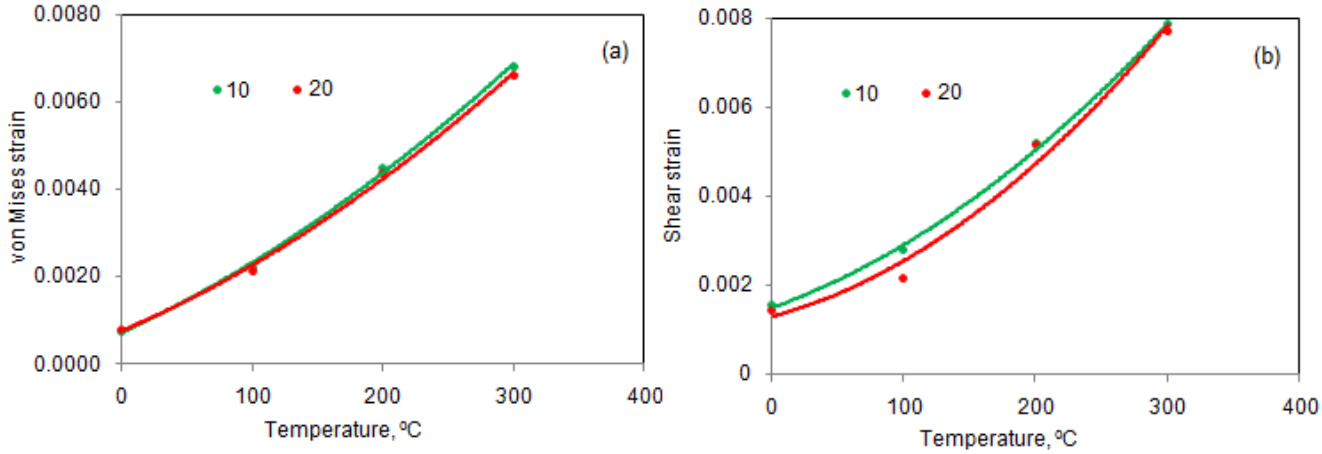

FIG. 10. INFLUENCE OF TEMPERATURE ON VON MISES STRESS.

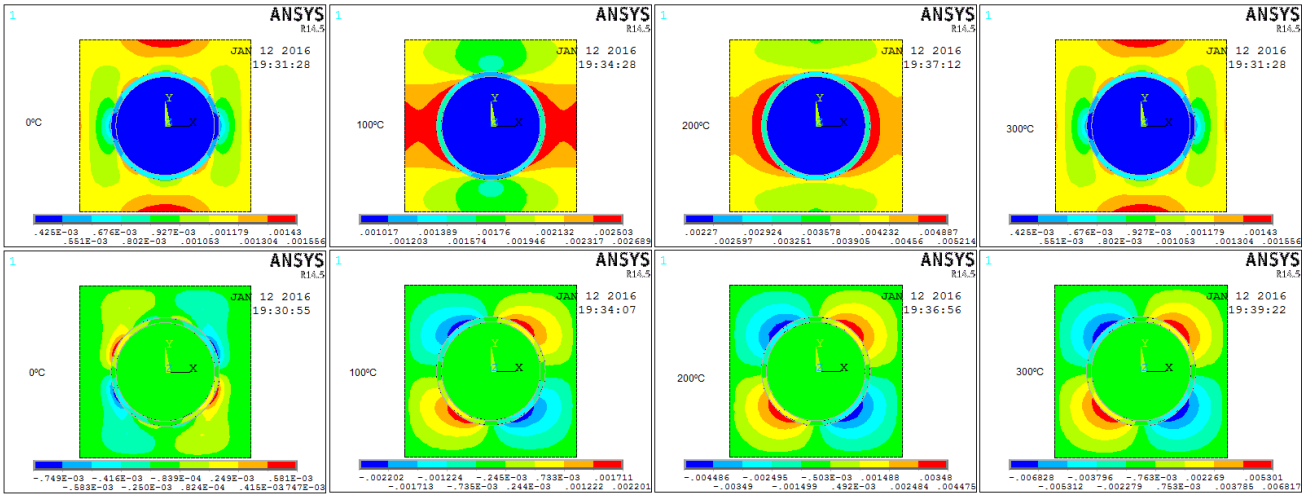

FIG. 11. RASTER IMAGES OF STRAINS OF AA6070/10%ZrO_2 COMPOSITES: (A) VON MISES AND (B) SHEAR.

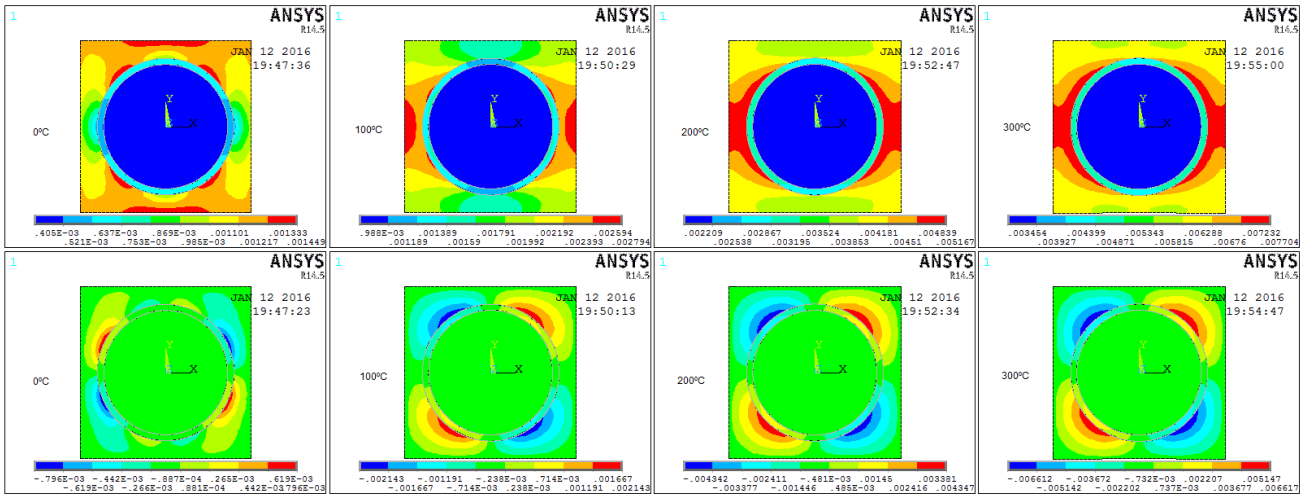

FIG. 12. RASTER IMAGES OF STRAINS OF AA6070/20%ZrO_2 COMPOSITES: (A) VON MISES AND (B) SHEAR.

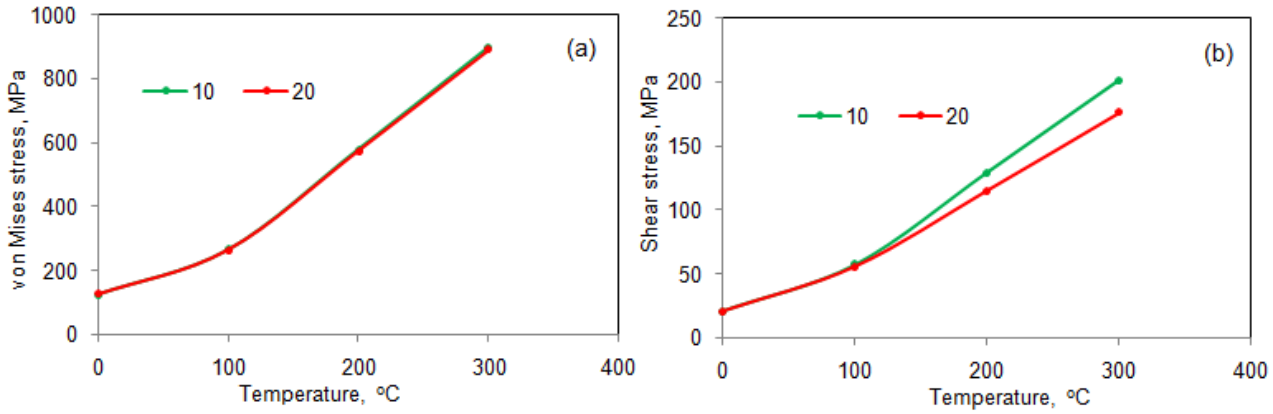

FIG. 13. INFLUENCE OF TEMPERATURE ON VON MISES STRESS.

Fig. 13(a) describes the von Mises stress induced in the composites. The von Mises stress increased with the increase of temperature from 0°C to 300°C. The von Mises stress was higher in the composites having 10% ZrO_2 nanoparticles than that in the composites consisting of 20% ZrO_2. The same kind of trend was observed with the shear stress as illustrated in Fig. 13(b).

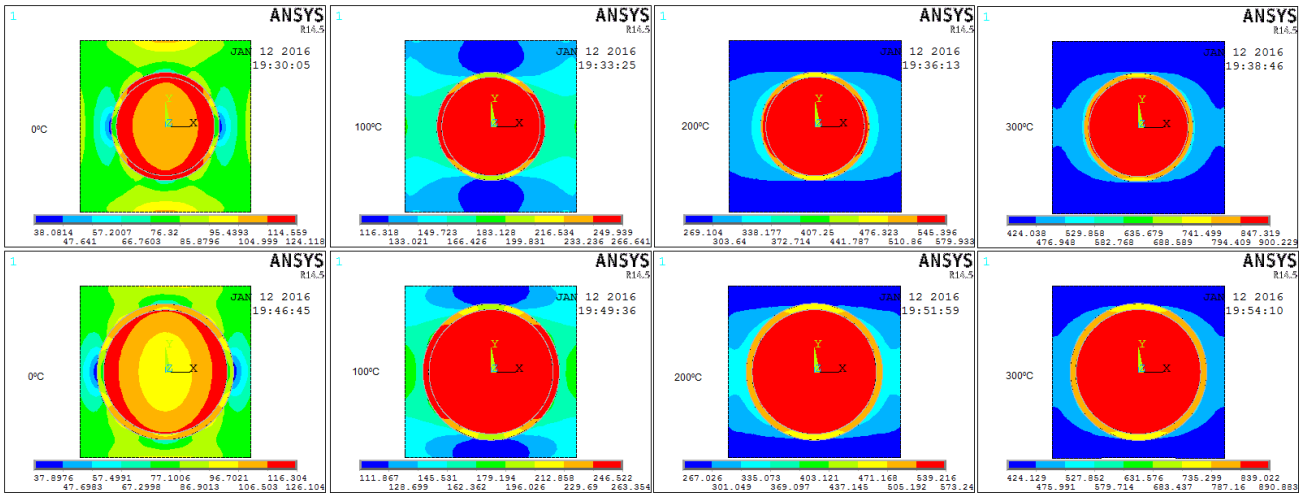

FIG. 14. RASTER IMAGES OF VON MISES STRESS AA6070/ZrO_2 COMPOSITES: 10% ZrO_2 AND (B) 20% ZrO_2.

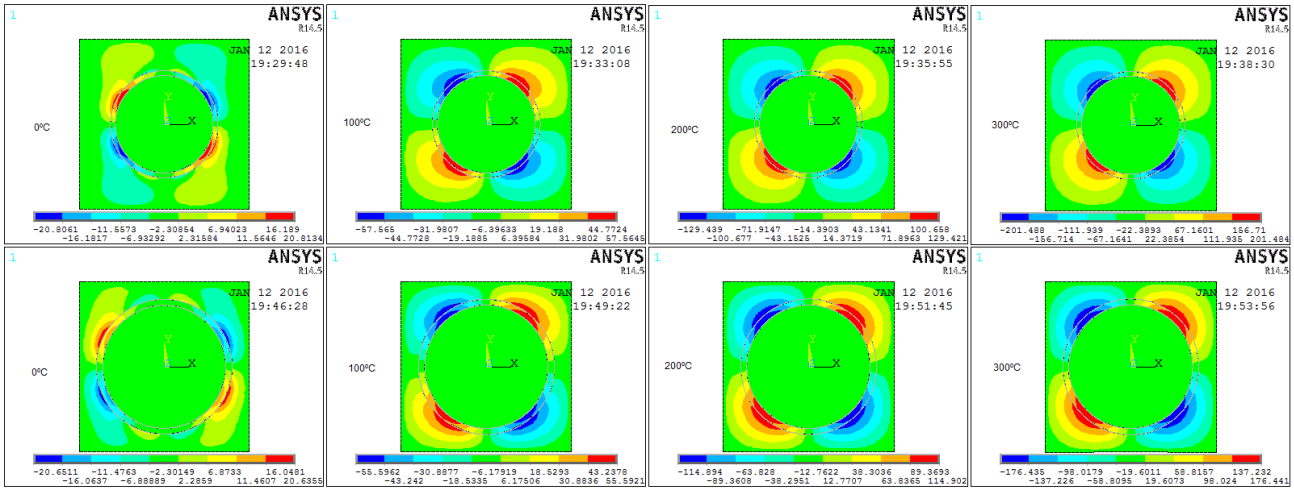

FIG. 15. RASTER IMAGES OF SHEAR STRESS OF STRESS AA6070/ZrO_2 COMPOSITES: 10% ZrO_2 AND (B) 20% ZrO_2

In the ZrO_2 nanoparticles, the von Mises stresses were higher than their tensile strength (711 MPa) at temperature 300^{o}C. This indicates the experience of thermal shock by the ZrO_2 nanoparticles at and above 300^{o}C. Fortunately, the ZrO_2 nanoparticles were not damaged because the interphase was sheared at all temperatures (figure 15).

IV. CONCLUSION

The thermoelastic strains and stresses increased with the increase of temperature. The stiffness decreased with increase of temperature for AA6070 alloy/ZrO_2 nanoparticulate metal matrix composites. ZrO_2 nanoparticles had experienced thermal shock at 300^{o}C. The fracture was observed at the interphase between AA6070 alloy and ZrO_2 nanoparticles.

REFERENCES

[1] A. C. Reddy, "Tensile properties and fracture behavior of 6063/SiCP metal matrix composites fabricated by investment casting process," International Journal of Mechanical Engineering and Materials Sciences, vol.03, no.01, pp.73-78, 2010.

[2] A. C. Reddy, "Experimental Evaluation of Elastic Lattice Strains in the Discontinuously SiC Reinforced Al-alloy Composites," National Conference on Emerging Trends in Mechanical Engineering, Nagapur, 05-06th February, 2004.

[3] A. C. Reddy, "Influence of strain rate and temperature on superplastic behavior of sinter forged Al6061/SiC metal matrix composites," International Journal of Engineering Research & Technology, vol.04, no.02, pp.189-198, 2011.

[4] A. C. Reddy and B. Kotiveerachari, "Influence of microstructural changes caused by ageing on wear behaviour of Al6061/SiC composites," Journal of Metallurgy & Materials Science, vol. 53, pp. 01, pp. 31-39, 2011.

[5] A. C. Reddy, "Cause and Catastrophe of Strengthening Mechanisms in 6063/Al_2O_3 Composites Prepared by Stir Casting Process: Validation through FEA," International Journal of Scientific & Engineering Research, vol. 06, no. 03, pp. 75-83, 2015.

[6] A. C. Reddy and Essa Zitoun, "Matrix al-alloys for alumina particle reinforced metal matrix composites," Indian Foundry Journal, vol.55, no.01, pp.12-16, 2009.

[7] A. C. Reddy, "Studies on fracture behavior of brittle matrix and alumina trihydrate particulate composites," Indian Journal of Engineering & Materials Sciences, vol.09, no.05, pp.365-368, 2002.

[8] A. C. Reddy, "Effects of Adhesive and Interphase Characteristics between Matrix and Reinforced Nanoparticle of AA2124/AlN Nanocomposites: Mathematical and Experimental Validation," International Journal of Engineering and Advanced Technology, vol. 5, no. 1, pp. 5-12, 2015.

[9] T. Prasad and A. C. Reddy, "Effects of Adhesive Characteristics between Matrix and Reinforced Nanoparticle of AA6061/Carbon Black Nanocomposites," International Journal of Scientific & Engineering Research, vol. 6, no. 7, pp. 40-45, 2015.

[10] A. C. Reddy, "Analysis of the relationship between the interface structure and the strength of carbon-aluminum composites, NATCON-ME, Bangalore, 13-14th March 2004.

[11] P.M. Hazzledine, "Direct versus indirect dispersion hardening," Scripta Metall. Mater., vol. 26, pp. 57-58, 1992.

[12] Y. Estrin, "Dislocation-density-related constitutive modeling," in: A.S. Krausz, K. Krausz (Eds.), Unified Constitutive Laws of Plastic Deformation, Academic Press, New York, 1996.

[13] C.R. Alavala, "Finite element Mehods: basic Concepts and Applications," PHI Learning Pvt. Ltd., New Dlehi, 2008.

[14] B. M. Lempriere "Poisson's ratio in orthotropic materials" AIAA Journal, vol. 6, no. 11, pp.2226-2227, 1968.